Magnetic moments of 2_1^+ states in ^{124,126,128}Sn

J. M. Allmond,[1] A. E. Stuchbery,[2] D. C. Radford,[3] A. Galindo-Uribarri,[3,4] N. J. Stone,[4,5] C. Baktash,[3,*] J. C. Batchelder,[6] C. R. Bingham,[3,4] M. Danchev,[7] C. J. Gross,[3] P. A. Hausladen,[1] K. Lagergren,[1] Y. Larochelle,[4] E. Padilla-Rodal,[1,†] and C.-H. Yu[3]

[1]*Joint Institute for Heavy Ion Research, Oak Ridge National Laboratory, Oak Ridge, Tennessee 37831, USA*
[2]*Department of Physics, Australian National University, Canberra ACT 0200, Australia*
[3]*Physics Division, Oak Ridge National Laboratory, Oak Ridge, Tennessee 37831, USA*
[4]*Department of Physics and Astronomy, University of Tennessee, Knoxville, Tennessee 37996, USA*
[5]*Department of Physics, Oxford University, Oxford OX1 3PU, United Kingdom*
[6]*UNIRIB, Oak Ridge Associated Universities, Oak Ridge, Tennessee 37831, USA*
[7]*Faculty of Physics, St. Kliment Ohridski University of Sofia, BG-1164 Sofia, Bulgaria*

(Received 3 April 2013; revised manuscript received 30 April 2013; published 20 May 2013)

The g factors of the first-excited states of stable ^{124}Sn and radioactive ^{126,128}Sn were measured by the recoil-in-vacuum method with comparatively high precision. The experiments were performed at the Holifield Radioactive Ion Beam Facility by Coulomb exciting ∼3 MeV/u beams in inverse kinematics on carbon and titanium targets. The results for ^{124}Sn and ^{126}Sn are in excellent agreement with recent shell-model calculations. For ^{128}Sn the experiment suggests an increase in the magnitude of $g(2_1^+)$, as predicted by some models. The present results provide a sensitive probe of the valence orbitals that contribute to the 2_1^+ wave functions as the double-shell closure at ^{132}Sn is approached.

DOI: 10.1103/PhysRevC.87.054325 PACS number(s): 21.10.Ky, 23.20.En, 25.70.De, 27.60.+j

I. INTRODUCTION

The Sn isotopes are of special interest in that they constitute the longest semimagic isotope chain available for nuclear structure study between double-magic ^{100}Sn ($N = Z = 50$) and double-magic ^{132}Sn ($Z = 50$, $N = 82$). Several theoretical approaches [1–4] have predicted the magnetic moments (or g factors) of 2_1^+ states in the Sn isotopes. The signs and magnitudes of the experimental g factors are sensitive to the valence orbitals that determine the 2_1^+ state wave functions. In particular, the contribution of the $\nu d_{3/2}$ and $\nu h_{11/2}$ configurations to the wave function significantly impacts the sign and magnitude of the 2_1^+-state g factors of isotopes toward ^{132}Sn. However, the experimental data have remained incomplete for the radioactive species approaching the ^{100}Sn and ^{132}Sn double-shell closures. There have been previous measurements on the stable Sn isotopes [5–7] and a recent transient-field measurement on neutron-rich ^{126}Sn, performed at the Holifield Radioactive Ion Beam Facility (HRIBF) [8], which determined the sign of the g factor to be negative.

Recently, we reported on the electric quadrupole transition strengths $B(E2; 0_1^+ \rightarrow 2_1^+)$ and electric quadrupole moments $Q(2_1^+)$ for stable ^{124}Sn and radioactive ^{126}Sn and ^{128}Sn isotopes provided by HRIBF. These nuclei were Coulomb excited as ∼3 MeV/u beams in inverse kinematics on carbon and titanium targets [9]. In the present study, the angular correlation data are analyzed to determine the magnitude of the gyromagnetic ratios, $g(2_1^+)$, using the recoil-in-vacuum (RIV) method [10–12]. This work represents the second and third examples of g-factor measurements on radioactive beams by the RIV method. It is demonstrated that the technique remains valid, giving experimental g factors with useful precision, as the 2^+-level lifetime becomes shorter (around 1 ps) and the attenuation effect becomes correspondingly smaller. It will be seen that the RIV result for ^{126}Sn is much more precise than the transient-field measurement on that isotope. Moreover, the precision of the present RIV measurement on ^{126}Sn is better than most of the previous transient-field measurements on the stable isotopes [5,6].

II. EXPERIMENT

When a free ion moves through vacuum the hyperfine interaction couples the atomic spin $\boldsymbol{J}$ to the nuclear spin $\boldsymbol{I}$ and together they precess about the total spin $\boldsymbol{F} = \boldsymbol{I} + \boldsymbol{J}$ at a frequency that is proportional to the nuclear g factor and the magnitude of the hyperfine magnetic field at the nucleus. To measure the g factor, the nucleus is excited and then allowed to recoil into vacuum. The effect of the hyperfine interaction is observed via the reduced anisotropy of the angular correlation of the γ rays deexciting the state of interest.

In the presence of vacuum deorientation, the particle-γ angular correlation after Coulomb excitation takes the form (see, e.g., Ref. [13] and references therein)

$$W(\theta_p, \theta_\gamma, \Delta\phi) = 1 + \sum_{kq} B_{kq}(\theta_p) Q_k G_k F_k D^{k*}_{q0}(\Delta\phi, \theta_\gamma, 0), \tag{1}$$

where θ_p and θ_γ are the polar detection angles for particles and γ rays, respectively. $\Delta\phi = \phi_\gamma - \phi_p$ is the difference between the corresponding azimuthal detection angles. The attenuation coefficients G_k specify the vacuum deorientation

[*]Present Address: U.S. Department of Energy.
[†]Present Address: Instituto de Ciencias Nucleares, UNAM, AP 70-543, 04510 México, D.F., México.

effect; $B_{kq}(\theta_p)$ is the statistical tensor, which defines the spin alignment of the initial state. F_k represents the usual F coefficient for the γ-ray transition, and Q_k is the attenuation factor for the finite size of the γ-ray detector. $D^{k*}_{q0}(\Delta\phi, \theta_\gamma, 0)$ is the rotation (Wigner-D) matrix, which is equivalent to a spherical harmonic in the present form. For $E2$ excitation, the "rank" k is $k = 2, 4$ and $-k \leqslant q \leqslant k$.

The experimental details, particle identifications, and γ-ray spectra have been given in Ref. [9]. Three "rings" of the "bare" HyBall array (BareBall) [14] (ring $2 = 14°$–$28°$, ring $3 = 28°$–$44°$, and ring $4 = 44°$–$60°$), and three "rings" of the CLARION array [15] (five Compton suppressed "Clover" detectors at 90°, four at 132°, and two at 154°) were used to construct nine particle-γ angular correlations in $\Delta\phi$. (Detection angles are given in the laboratory frame with respect to the beam axis.) The attenuations of these nine angular correlations were used to determine $|g|\tau$, where g is the gyromagnetic ratio and τ is the mean lifetime of the 2^+_1 state.

III. ANALYSIS AND CALIBRATION PROCEDURES

In previous work [10,11], the RIV g-factor measurement consisted of first determining the attenuation coefficients G_2 and G_4 from fits to experimental angular correlations and, second, determining $|g|\tau$ from the G_k values by means of a calibration curve like that in Fig. 1. The analysis procedure largely follows that described previously. However, for the weak radioactive beams studied here, the relatively low statistical precision of the data makes a two-step analysis impractical. Therefore, $|g|\tau$ was determined directly from fits to the angular correlations by expressing the attenuation coefficients as a function of $|g|\tau$; the single parameter $|g|\tau$ determines both G_2 and G_4. Another complication in the present work is that the recoil velocity of the Sn ions varies

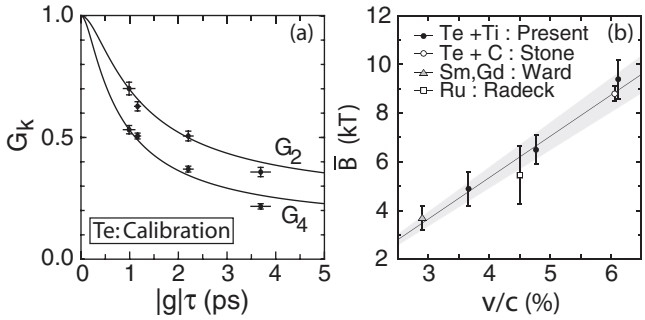

FIG. 1. Calibration of free-ion hyperfine interaction for $_{50}$Sn is based on data for $_{52}$Te (see text). (a) Attenuation coefficients versus $|g|\tau$. Data are for ^{132,130,126,122}Te (left to right) recoiling into vacuum with $v/c \sim 0.06$. The curve is a model-based parametrization which depends on $\bar{B}$, the average hyperfine field at the nucleus [11]. These calibration data are representative for the data taken with the C target, and for BareBall ring 4 with the Ti target. (b) Dependence of the average hyperfine field on velocity extracted from RIV data for Te ions recoiling into vacuum from Refs. [10,11] and the present work. Fields for Ru, and Sm and Gd ions were obtained from a reanalysis of the results of Radeck *et al.* [16] and Ward *et al.* [17], respectively.

with the scattering angle (strongly so for the Ti target), and hence the BareBall ring number. The consequent variation of the strength of the hyperfine fields with scattering angle must be included in the analysis; there is a separate G_k vs $|g|\tau$ curve for each beam, target, and BareBall detection ring.

A procedure to characterize G_k in terms of the ion velocity and $|g|\tau$ has therefore been developed, based on extensive comparisons between experimental data and model-based calculations [11,12]. In the static model of the RIV interaction, as described by Stuchbery and Stone [11], the observed G_k value is a superposition of the attenuation coefficients for a distribution of many individual electronic configurations with spin J_i and hyperfine field B_j, denoted $G_k(J_i, B_j, |g|\tau)$. The distribution of such atomic states is parametrized by normalized Gaussian distributions, w_J and w_B, which represent the distribution of electronic spins and hyperfine fields, respectively. Thus

$$G_k = \sum_{i,j} w_J(J_i) w_B(B_j) G_k(J_i, B_j, |g|\tau). \tag{2}$$

For nuclear spin $I = 2$, the G_k become insensitive to the precise value of $\bar{J}$ once $\bar{J} > 2$ [12,18]. As a consequence, for nuclei in the vicinity of $Z = 50$, the average atomic spin can be set to $\bar{J} = 4.5$ [11]. In general, there is little sensitivity to the width of the spin distribution, making it possible to set $\sigma_J = 1$ universally. Along with the data near $Z = 50$ discussed here, good fits to experimental G_k values are obtained for $_{32}$Ge and $_{34}$Se ions with the model of Eq. (2). Moreover, the data in both regions are well described by setting the width of the field distribution σ_B equal to the mean field, $\bar{B}$; see Refs. [11,12,18]. It has thus proved possible to describe the RIV data near $Z = 50$ in terms of the single parameter $\bar{B}$. The velocity dependence of $\bar{B}$ can therefore be used to characterize the velocity dependence of the G_k attenuation coefficients.

The dependence of $\bar{B}$ on the ion velocity was determined by fitting Eq. (2) to experimental data. The results of Stone *et al.* [10] for 3 MeV/u ^{122,126,130}Te scattered from carbon targets were combined with additional measurements on 390 MeV (3.1 MeV/u) ^{126}Te scattered from a 1.5 mg/cm^2 ^{50}Ti target (again using the BareBall and CLARION arrays). The resulting variation of the average field with ion velocity is shown in Fig. 1(b). This analysis adopted g factors of ^{122,126,130}Te from Ref. [19] and lifetimes from Raman *et al.* [20]. To analyze the angular-correlation data taking account of the differences in ion velocity for each beam, target, and particle-detection angle, we adopt the linear parametrization of $\bar{B}$ versus v/c shown in Fig. 1(b). It can be noted that the G_k versus $|g|\tau$ curve in Fig. 1(a) approximates an average over all BareBall rings for the C target and is also close to the correct curve for BareBall ring 4 with the Ti target. For the other two rings and the Ti target, the curve differs markedly. For example, for ring 2 the G_4 curve is close to the G_2 line in Fig. 1(a), with the G_2 curve correspondingly closer to unity.

The average hyperfine fields for $_{50}$Sn and $_{52}$Te might differ somewhat for equivalent ion velocities. However, the Z dependence of the RIV fields in the domain of interest is

weak as is evidenced by the data for $_{44}$Ru, $_{62}$Sm, and $_{64}$Gd shown in Fig. 1(b). These ions all have $\bar{B}$ values that overlap the calibration curve for $Z = 52$. This weak dependence on Z comes from a trade off: the increase in hyperfine field with increasing Z for a given electronic configuration is offset by a change in charge state—the higher-Z ion carries more electrons (for a given v/c) which moderates the increase in hyperfine field. The available experimental data spanning $Z = 46$ to $Z = 64$, which are summarized in Fig. 1(b), are consistent with a Z-independent hyperfine interaction in the regime of interest. RIV measurements on the lower-Z ions $_{32}$Ge and $_{34}$Se ions recoiling into vacuum with $v/c \sim 0.05$ have a smaller average field than in Fig. 1(b), but the measured attenuation coefficients for these two ions are consistent with both having the same average hyperfine field strength [12]. It is well justified, therefore, to consider the average hyperfine fields for Sn and Te equal, well within the precision of the measurements.

The shaded region in Fig. 1(b) represents an uncertainty of $\pm 8\%$, which is assigned to the field calibration parameter $\bar{B}$. This uncertainty originates about equally from the uncertainties in the adopted g factors in Ref. [19] (absolute uncertainty of approximately $\pm 6\%$) and the experimental uncertainties in the G_k values from the RIV calibration measurements. The uncertainty in $\bar{B}$ must be propagated through the G_k calibration curves to the g factor. In the static-field approximation, the dependence of the attenuation coefficients on $|g|$, τ, and B is always in terms of the product $|g|\tau B$. Consequently, the $\pm 8\%$ uncertainty in $\bar{B}$ becomes a $\pm 8\%$ uncertainty in $|g|\tau$, which can be added in quadrature with the statistical uncertainty.

The present g-factor measurements require an extrapolation of the G_k versus $|g|\tau$ curves toward $|g|\tau = 0$. Extensive modeling—together with detailed experimental studies of the RIV free-ion hyperfine interactions, as discussed in Refs. [11,12]—gives confidence in the reliability of an extrapolation based on Eq. (2). In particular, the curve is strongly constrained because (i) $G_k \to 1$ as $|g|\tau \to 0$, (ii) the functional form of G_k must approach an inverted parabola as $|g|\tau \to 0$, and (iii) atomic transitions strongly affect the 'hard core' value of G_k at long times, but have little influence near $\tau = 0$ [11,12,21]. It is relevant to note that the adopted calibration and extrapolation procedure accurately predicts the G_k values for ^{70}Ge and ^{72}Ge, having $|g|\tau = 0.88$ ps and $|g|\tau = 1.83$ ps, respectively, based on a fit to the experimental G_k versus $|g|\tau$ data for Se ions having $|g|\tau \geqslant 4.37$ ps [12].

IV. RESULTS

Experimental angular correlations for the C target are displayed in Figs. 2–4. The angular correlations for both the C and Ti targets have been given in a preliminary account of this work [22]. For a given BareBall and CLARION ring, the coincidence count for a particular BareBall segment and γ-ray detector was first normalized to the Rutherford scattering yield to account for any variations in efficiency of the BareBall elements. The efficiency of the γ-ray detector was factored out by normalizing the coincidence counts in a chosen pair of

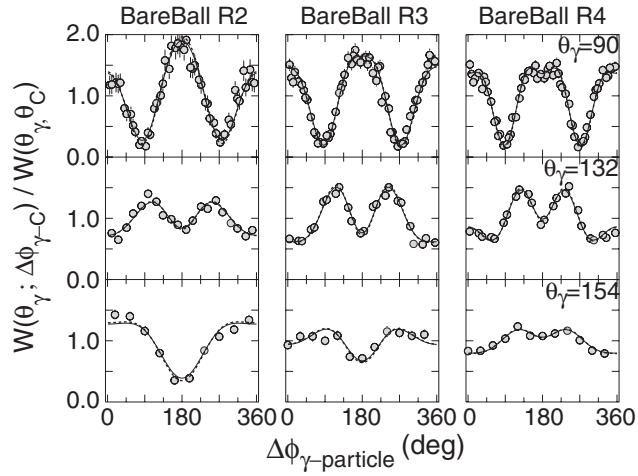

FIG. 2. Angular correlations for ^{124}Sn excited on C. The unperturbed correlation is shown by the dashed curve; solid lines show the attenuated correlations.

particle and γ-ray detectors, $N(\theta_p, \theta_\gamma, \phi_\gamma - \phi_{p_i})$, to the sum over all particle detector segments in the particular BareBall ring:

$$\frac{N_H N(\theta_p, \theta_\gamma, \phi_\gamma - \phi_{p_i})}{\sum_i N(\theta_p, \theta_\gamma, \phi_\gamma - \phi_{p_i})} = \frac{W(\theta_p, \theta_\gamma, \phi_\gamma - \phi_{p_i})}{W(\theta_p, \theta_\gamma)}. \quad (3)$$

N_H is the number of detectors in the BareBall ring and $W(\theta_p, \theta_\gamma)$ is given by Eq. (1) with $q \equiv 0$. By this procedure, the only free parameters required to fit the perturbed angular correlations are the vacuum attenuation factors, G_2 and G_4, which are set by the value of $|g|\tau$.

Experimental results are presented in Tables I–III. The small attenuations are hard to discern by inspection of the angular correlations alone, however, the plots of χ^2 versus $|g|\tau$ in Fig. 5 all show a clear minimum for $|g|\tau > 0$.

The χ^2 per degree of freedom in the fits is typically $\chi^2_\nu \sim 1.3$, a little greater than unity. The error estimates from the χ^2 fits have all been increased by $\sqrt{\chi^2_\nu}$. By modeling the detector arrangement and examining high-statistics angular

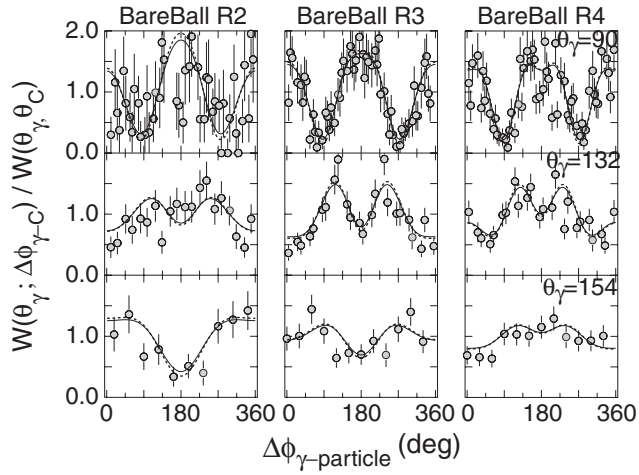

FIG. 3. Angular correlations for ^{126}Sn on C.

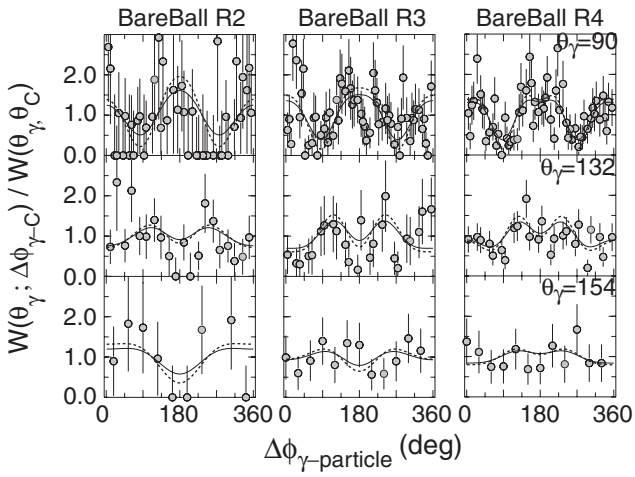

FIG. 4. Angular correlations for ^{128}Sn on C.

correlations measured with stable beams, it has been inferred that any small misalignment of BareBall with respect to the beam axis will increase χ^2. However, because the CLARION-BareBall arrays have a high degree of axial symmetry, the $|g|\tau$ value at the χ^2 minimum is robust against such small misalignments.

Table I shows detailed results for the stable-beam case, ^{124}Sn. For each BareBall ring the best fit values of $|g|\tau$ are shown, along with the corresponding G_k values. The uncertainties in Table I are statistical only. There is excellent consistency between the six independent measurements of $|g|\tau$ for ^{124}Sn, which span the velocity range from $v/c = 0.037$ (average charge state $\bar{q} \sim 22+$; mainly Zn-like ions) to $v/c = 0.065$ ($\bar{q} \sim 31+$; mainly Sc-like ions). The high level of consistency among all six extracted $|g|\tau$ values for ^{124}Sn shown in Table I gives confidence in analysis procedures and in the adopted extrapolation of the G_k calibration curves towards $|g|\tau = 0$.

Table II summarizes the $|g|\tau$ values extracted for ^{124,126,128}Sn. Like the case of ^{124}Sn, the data for ^{126}Sn for the C and Ti targets give $|g|\tau$ values in excellent agreement. For ^{128}Sn the results for the two targets are consistent only at the 2σ level. Given the consistency of the data sets for ^{124}Sn and ^{126}Sn,

TABLE I. Angular-correlation fits for ^{124}Sn by target and BareBall ring number. The data and analysis procedure show remarkable consistency.

Target	Ring	v/c	G_2	G_4	$\|g\|\tau$ (ps)
C	2	0.059	0.987 (7)	0.96 (2)	0.12 (4)
	3	0.062	0.979 (7)	0.94 (2)	0.15 (3)
	4	0.066	0.975 (8)	0.93 (2)	0.15 (3)
	2–4				0.145 (19)[a]
Ti	2	0.037	0.995 (4)	0.98 (1)	0.13 (6)
	3	0.049	0.988 (4)	0.96 (1)	0.15 (3)
	4	0.060	0.982 (7)	0.95 (2)	0.14 (3)
	2–4				0.142 (20)[a]

[a]Global fit for BareBall rings 2–4.

TABLE II. Summary of $|g|\tau$ results for ^{124,126,128}Sn by target.

Nuclide	$\|g\|\tau$ (ps)[a]		
	C target	Ti target	Combined fit
^{124}Sn	0.145 (19)	0.142 (20)	0.143 (13)
^{126}Sn	0.21 (6)	0.18 (6)	0.193 (45)
^{128}Sn	0.82 (24)	0.32 (15)	0.55 (12)

[a]Statistical error only (uncertainty in hyperfine field not included).

which were measured and analyzed by the same procedures, this difference most likely stems from the lower statistical precision of the ^{128}Sn data set wherein the number of counts for a given particle-gamma coincidence is $\leqslant 11$. For such low counts, Poisson statistics should be applied and a chi-squared fit may not be appropriate. However, a maximum likelihood analysis of the ^{128}Sn data set, based on Poisson statistics, gave the same best fit value as the chi-squared analysis. In view of this agreement, the $|g|\tau$ values from the global chi-squared fits to the data for both targets, shown in the last column of Table II, are adopted to extract the g factors.

The lifetimes from the $B(E2; 0_1^+ \rightarrow 2_1^+)$ values in Ref. [9] and the g-factor results from the present study are summarized in Table III. Transient-field measurements [5,7,8] have determined the signs of the g factors in ^{124}Sn and ^{126}Sn. Whereas the experimental trend in $g(2_1^+)$ and most theories (see below) would suggest $g < 0$ for ^{128}Sn, the RIV measurement does not determine the sign. A positive g factor for ^{128}Sn cannot be excluded.

V. DISCUSSION

A. Comparisons with previous work

Experimental results are compared with previous measurements and recent theoretical calculations in Fig. 6. Overall, the present RIV measurements agree well with the previous transient-field measurements. For ^{124}Sn the precision of the RIV measurement is much better than the measurements of Hass *et al.* [5], East *et al.* [6], and Kumbartzki *et al.* [8]; the precision is comparable to the measurement of Walker *et al.* [7]. The RIV measurement favors a larger magnitude for the g factor of ^{124}Sn than the TF measurement of Walker *et al.* However, with a ratio of $g(\text{RIV})/g(\text{TF}) = 1.6 \pm 0.4$, the values are consistent within two standard deviations.

TABLE III. Summary of g-factor results for ^{124,126,128}Sn.

A	τ (ps)[a]	$\|g\|\tau$ (ps)[b]	$g(2_1^+)$[c]
124	1.35 (5)	0.143 (17)	−0.106 (13)
126	1.66 (10)	0.19 (5)	−0.12 (3)
128	2.35 (15)	0.55 (13)	(−)0.23 (6)

[a]Lifetimes taken from $B(E2; 0_1^+ \rightarrow 2_1^+)$ values in Ref. [9].
[b]Includes uncertainty in hyperfine field calibration.
[c]Signs adopted from transient-field measurements [5,7,8] for ^{124,126}Sn and from systematics for ^{128}Sn.

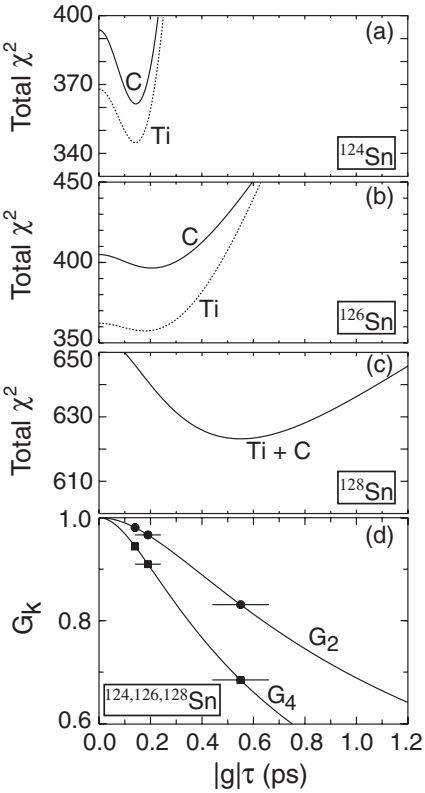

FIG. 5. Total χ^2 versus $|g|\tau$ for (a) ^{124}Sn, (b) ^{126}Sn, and (c) ^{128}Sn. (d) Best fit $|g|\tau$ values for each isotope and their uncertainties, projected onto the relevant part of the G_k-versus-$|g|\tau$ calibration curves from Fig. 1(a).

B. Free-ion hyperfine interaction calibration

Some comments on the procedure used to calibrate the hyperfine interactions are in order. We discuss in turn (i) the limitations of simple empirical characterizations of the attenuation coefficients for measurements on short-lived states, (ii) the impact of including atomic transitions in the modeling used to calibrate and extrapolate the hyperfine interactions, and (iii) comparisons between the model-based empirical fits used here and recent *ab initio* calculations by Chen *et al.* [21].

(i) A simple empirical extrapolation of the G_k versus $|g|\tau$ curve from the G_k data near $|g|\tau = 1$ for ^{130}Te, toward $G_k = 1$ at $|g|\tau = 0$, was not used in the present study on short-lived excited states of the Sn isotopes. In previous work, where $|g|\tau \gtrsim 1$, the assumption of an exponential time dependence for the attenuation factors has proven useful [11,12,16]. However, employing such an approach for cases near to $|g|\tau = 0$ is not physical. It is important to recognize that such an approach cannot be used here, especially for ^{124}Sn, where the extracted g factor would decrease by about a factor of two. A more complex procedure is needed because there is no simple empirical formula that makes the necessary transition from the inverted parabolic behavior of the attenuation coefficients near time zero to their quasi-exponential behavior at longer times.

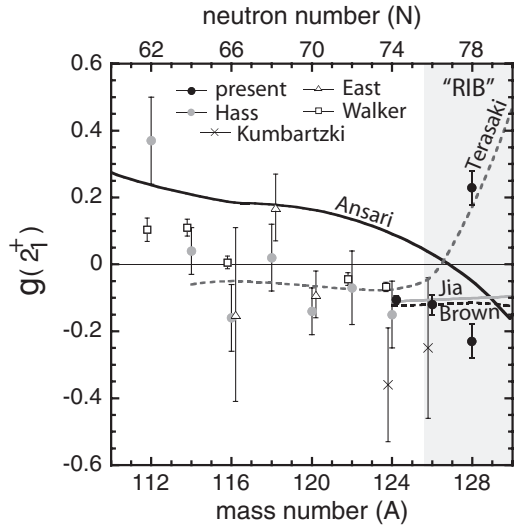

FIG. 6. Experimental (present study, Hass *et al.* [5], East *et al.* [6], Walker *et al.* [7], and Kumbartzki *et al.* [8]) and theoretical (Terasaki *et al.* [1], Brown *et al.* [2], Ansari *et al.* [3], and Jia *et al.* [4]) g factors of 2_1^+ states in the even Sn isotopes.

(ii) The static-model fit used to describe the relevant free-ion hyperfine interactions has the correct parabolic shape near time zero, followed by a quasi-exponential decay. However, it is expected that there will be some atomic transitions on the time scale of the nuclear decay. The impact of these fluctuations on the G_k versus $|g|\tau$ curve has been investigated for the calibration data on the Te isotopes [11,12]. In the present study, the effect of including atomic transitions would be to increase the extracted g factors, but by a negligible fraction of the experimental uncertainty; see Fig. 7 of Ref. [12].

(iii) Very recently Chen *et al.* [21] have reported calculations of the attenuation coefficients for the Te isotopes based on atomic calculations. They adjusted the number of electronic excitations in their calculations to best reproduce the experimental attenuation coefficients for ^{122}Te, the calibration isotope with the longest 2_1^+-level lifetime, and hence the largest $|g|\tau$ value. Here, the priority was to fit the calibration isotope with the shortest 2_1^+-level lifetime, ^{130}Te. Once these differences are taken into account, the calibration of the hyperfine interaction used here conforms closely to that obtained by the microscopic atomic calculations of Chen *et al.* Importantly, their *ab initio* calculations confirm that the G_k curve follows a parabolic shape near $|g|\tau = 0$.

In the future, fully *ab initio* calculations of the required free-ion hyperfine interactions may be possible, thus removing the need to resort to empirical calibration procedures. However, at present the main obstacle to truly *ab initio* calculations is that the initial population of the the atomic states as the ion enters into vacuum is not well known [12]. Nevertheless, the extensive "toy-model" calculations of Stuchbery and Stone [11], together with the detailed atomic calculations of Chen *et al.* [21], demonstrate that the procedures used here to calibrate the hyperfine fields are reliable. The uncertainty in the

calibration of the hyperfine interactions is thus dominated by the uncertainties in the g factors, level lifetimes, and measured attenuation coefficients, which give the $\pm 8\%$ uncertainty in the field parameter $\bar{B}$ discussed above.

C. Comparison with theory

Beginning with the quasiparticle random phase approximation (QRPA) calculations of Terasaki *et al.* [1], the g factors of the even Sn isotopes towards ^{132}Sn have been calculated in several theoretical approaches over the past decade. Terasaki *et al.* used a separable quadrupole-plus-pairing Hamiltonian to give the same interactions above and below the $N = 82$ shell gap. These calculations are alone in predicting a positive $g(2_1^+)$ in ^{128}Sn, which implies that the 2_1^+ state wave function is dominated by the $\nu d_{3/2}^2$ configuration.

The shell-model calculations of Brown *et al.* [2], with CD-Bonn residual interactions and the inclusion of core polarization and meson-exchange corrections to the $M1$ operator, are the most microscopic calculations to date. These calculations predict relatively constant negative g factors for the 2_1^+ states of ^{124,126,128,130}Sn, which is in good agreement with the magnitude of the observed g factors (particularly for ^{124}Sn and ^{126}Sn). The shell-model wave functions are mixed, not least because the $\nu d_{3/2}$ and $\nu h_{11/2}$ orbits are almost degenerate in the heavier Sn isotopes.

Jia *et al.* [4] used a collective S and D nucleon-pair approximation to the shell model, and also predict near-constant negative g factors of a magnitude that agrees with the shell-model calculations [2].

The relativistic quasiparticle random phase approximation (RQRPA) calculations of Ansari and Ring [3] cover the whole range of measured g factors. The general theoretical trend of $g(2_1^+)$ decreasing from $N = 112$ to $N = 130$ agrees with the experimental trend. However, the theory is more positive than the experimental values by a near-constant offset of $\sim$0.15. In contrast with the shell-model calculations, which have no explicit proton contribution to wave function, the RQRPA calculations include proton contributions explicitly. As discussed in Ref. [6], the g factors in the QRPA models are very sensitive to the proton orbital contribution, and the theory of Ansari and Ring [3] has a relatively large proton orbital contribution.

To broaden the comparison of theory and experiment, the g factors of the 2_1^+ states in the even Sn isotopes, and the g factors of the ground states and low-lying isomers ($11/2^-$ and $3/2^+$ states) in the odd-A isotopes were calculated in the shell model using the OXBASH code [23]. Isotopes from ^{124}Sn through to ^{131}Sn were included. The interactions of Brown *et al.* [2], which give the correct ordering of the $11/2^-$ and $3/2^+$ states in the odd-A Sn isotopes, were used. A simple $M1$ operator with $g_l = 0$ and $g_s = -2.52$ was used. Results are compared with experiment in Table IV. Assuming that the g factor in ^{128}Sn is negative, these shell-model calculations generally reproduce the experimental g factors very well. There are small differences in experimental and theoretical trends. For example, in the odd-A isotopes, the predicted increase in $g(3/2^+)$ with N is not observed. However, this difference is small compared to the overall good agreement between the shell model and experiment for states in both the even and odd isotopes.

TABLE IV. Shell-model g factors in even and odd Sn isotopes. Experimental values are from the present work and the compilation of Stone [24].

Nuclide	J^π	Theory	Experiment
^{124}Sn	2^+	-0.120	-0.106 (13)
^{125}Sn	$3/2^+$	$+0.440$	$+0.509$ (2)
	$11/2^-$	-0.224	-0.2451(4)
^{126}Sn	2^+	-0.117	-0.12 (3)
^{127}Sn	$3/2^+$	$+0.476$	$+0.505$ (3)
	$11/2^-$	-0.225	-0.242(1)
^{128}Sn	2^+	-0.113	$(-)0.23$ (6)
^{129}Sn	$3/2^+$	$+0.493$	$+0.503$ (4)
	$11/2^-$	-0.227	-0.236 (1)
^{130}Sn	2^+	-0.127	
^{131}Sn	$3/2^+$	$+0.504$	$+0.498$ (3)
	$11/2^-$	-0.219	-0.232 (1)

According to the shell-model calculations [2], the 2_1^+ wave function in ^{128}Sn includes $\nu d_{3/2}^2$ admixtures along with $\nu h_{11/2}^n$ contributions ($n = 8, 10$) which dominate to give an overall negative g factor. In contrast, Terasaki *et al.* [1] have a positive g factor because their QRPA wave function is dominated by the $\nu d_{3/2}^2$ configuration. A transient-field measurement on ^{128}Sn is needed to determine the sign of $g(2_1^+)$ and thus distinguish between these theoretical models.

In summary, the g factors of the first-excited states of stable ^{124}Sn and radioactive ^{126,128}Sn were measured with comparatively high precision (particularly for ^{124,126}Sn) by the recoil-in-vacuum method using both carbon and titanium targets. These new results were achieved by employing particle-γ coincidence spectroscopy with a CsI-HPGe array; this technique provides a powerful tool for future g-factor studies on radioactive ion beams in inverse kinematics. The different models make diverse predictions for the behavior of the 2_1^+-state g factors toward ^{132}Sn. The experimental g factors (sign and magnitude) for ^{124,126}Sn show excellent agreement with shell-model calculations by Brown *et al.* [2]. While the magnitude of the experimental g factor for ^{128}Sn is also consistent with the shell-model calculations by Brown *et al.*, the sign will need to be determined by a transient-field measurement to distinguish from the QRPA calculations of Terasaki *et al.* [1]. Such measurements should be feasible with the next generation of re-accelerated radioactive beam facilities.

ACKNOWLEDGMENTS

The authors thank the HRIBF operations staff for developing and providing the stable and radioactive beams used in this study. This research was sponsored by the Office of Nuclear Physics, US Department of Energy, and by the Australian Research Council grant No. DP0773273. This work was also supported in part by the US DOE under Contracts No. DE-AC05-76OR00033 (UNIRIB) and No. DE-FG02-96ER40963 (UTK).

[1] J. Terasaki, J. Engel, W. Nazarewicz, and M. Stoitsov, Phys. Rev. C **66**, 054313 (2002).
[2] B. A. Brown, N. J. Stone, J. R. Stone, I. S. Towner, and M. Hjorth-Jensen, Phys. Rev. C **71**, 044317 (2005).
[3] A. Ansari and P. Ring, Phys. Lett. B **649**, 128 (2007).
[4] L. Y. Jia, H. Zhang, and Y. M. Zhao, Phys. Rev. C **75**, 034307 (2007).
[5] M. Hass, C. Broude, Y. Niv, and A. Zemel, Phys. Rev. C **22**, 97 (1980).
[6] M. C. East, A. E. Stuchbery, A. N. Wilson, P. M. Davidson, T. Kibédi, and A. I. Levon, Phys. Lett. B **665**, 147 (2008).
[7] J. Walker *et al.*, Phys. Rev. C **84**, 014319 (2011).
[8] G. J. Kumbartzki *et al.*, Phys. Rev. C **86**, 034319 (2012).
[9] J. M. Allmond *et al.*, Phys. Rev. C **84**, 061303(R) (2011).
[10] N. J. Stone *et al.*, Phys. Rev. Lett. **94**, 192501 (2005).
[11] A. E. Stuchbery and N. J. Stone, Phys. Rev. C **76**, 034307 (2007).
[12] A. E. Stuchbery, Hyperfine Interact **220**, 29 (2013).
[13] A. E. Stuchbery, Nucl. Phys. A **723**, 69 (2003).
[14] A. Galindo-Uribarri, AIP Conf. Proc. **1271**, 180 (2010); www.phy.ornl.gov/hribf/research/equipment/hyball
[15] C. J. Gross *et al.*, Nucl. Instrum. Methods Phys. Res., Sect. A **450**, 12 (2000).
[16] D. Radeck *et al.*, Phys. Rev. C **85**, 014301 (2012).
[17] D. Ward, H. R. Andrews, R. L. Graham, J. S. Geiger, and N. Rud, Nucl. Phys. A **234**, 94 (1974).
[18] A. E. Stuchbery, J. Phys.: Conf. Ser. **387**, 012012 (2012).
[19] A. E. Stuchbery, A. Nakamura, A. N. Wilson, P. M. Davidson, H. Watanabe, and A. I. Levon, Phys. Rev. C **76**, 034306 (2007).
[20] S. Raman, C. W. Nestor, Jr., and P. Tikkanen, At. Data Nucl. Data Tables **78**, 1 (2001).
[21] X. Chen, D. G. Sarantites, W. Reviol, and J. Snyder, Phys. Rev. C **87**, 044305 (2013).
[22] A. E. Stuchbery *et al.*, in *Proceedings of Fifth International Conference on Fission and Properties of Neutron-Rich Nuclei (ICFN5), Sanibel Island, Florida, USA, November 2012*, edited by J. H Hamilton (World Scientific Publishing Company, Singapore, 2012).
[23] B. A. Brown, A. Etchegoyen, N. S. Godwin, W. D. M. Rae, W. A. Richter, W. E. Ormand, E. K. Warburton, J. S. Winfield, L. Zhao, and C. H. Zimmerman, Oxbash for Windows PC, Michigan State University, Report No. MSU-NSCL 1289 (2004).
[24] N. J. Stone, At. Data Nucl. Data Tables **90**, 75 (2005).